Journal Pre-proof

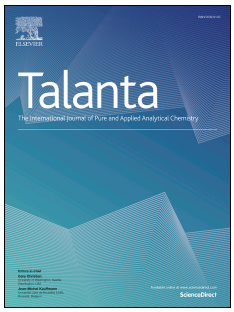

Differential-based biosensor array for fluorescence-chemometric discrimination and the quantification of subtle chloropropanols by cross-reactive serum albumin scaffolding

Siew Fang Wong, Kah Hin Low, Sook Mei Khor

PII: S0039-9140(20)30460-4

DOI: https://doi.org/10.1016/j.talanta.2020.121169

Reference: TAL 121169

To appear in: *Talanta*

Received Date: 31 March 2020

Revised Date: 8 May 2020

Accepted Date: 13 May 2020

Please cite this article as: S.F. Wong, K.H. Low, S.M. Khor, Differential-based biosensor array for fluorescence-chemometric discrimination and the quantification of subtle chloropropanols by cross-reactive serum albumin scaffolding, *Talanta*, https://doi.org/10.1016/j.talanta.2020.121169.

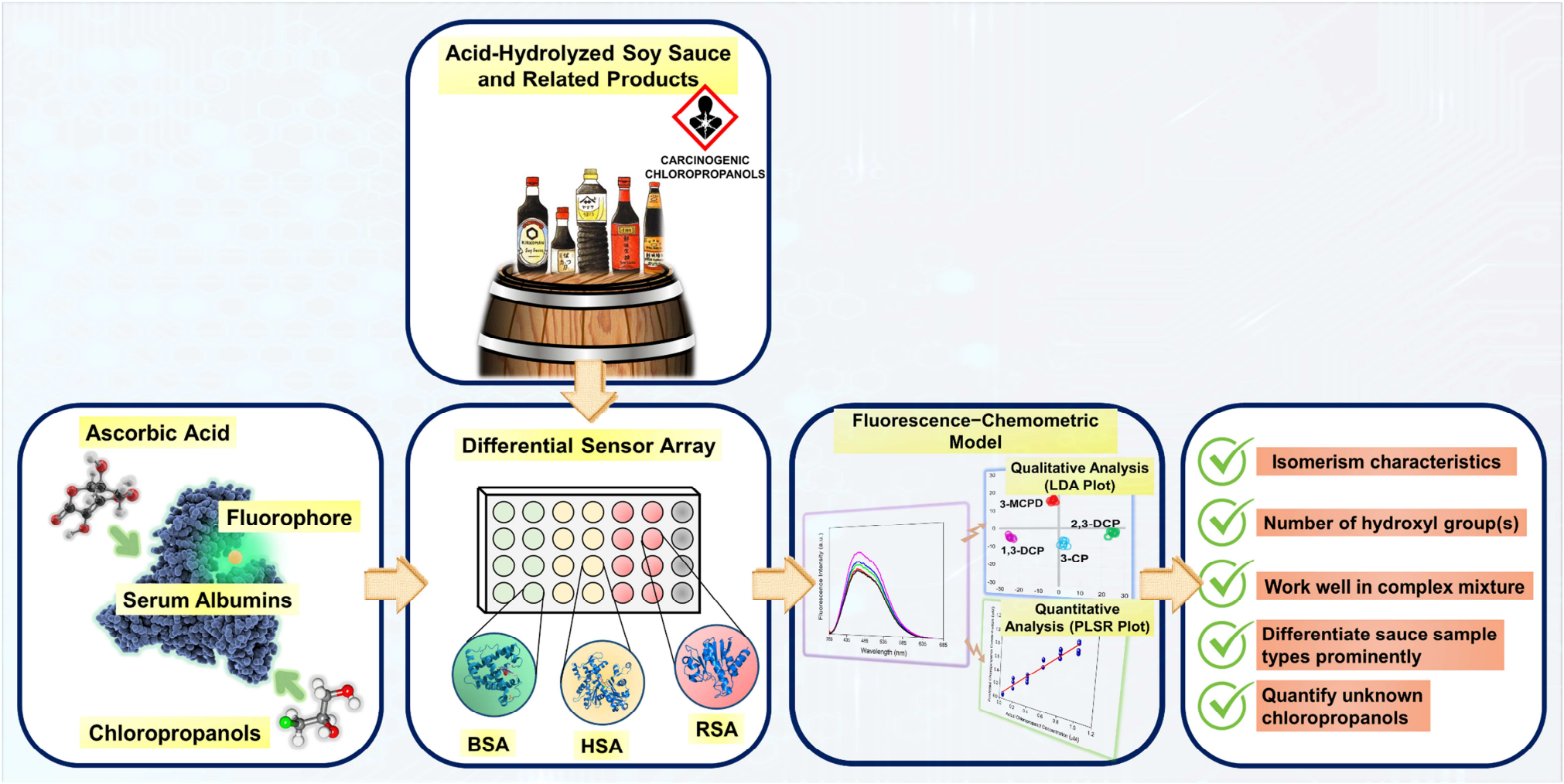

Graphical Abstract

Differential-based biosensor array for fluorescence-chemometric discrimination and the quantification of subtle chloropropanols by cross-reactive serum albumin scaffolding

Siew Fang Wong[a], Kah Hin Low[a], Sook Mei Khor[a,b,*]

[a] *Department of Chemistry, Faculty of Science, University of Malaya, 50603 Kuala Lumpur, Malaysia*

[b] *Centre for Innovation in Medical Engineering, Faculty of Engineering, University of Malaya, 50603 Kuala Lumpur, Malaysia*

* Corresponding author.

E-mail address: naomikhor@um.edu.my (S.M. Khor).

Tel: +603-7967 7022, Ext. 2520; Fax: +603-7967 4193.

ABSTRACT

Food contamination is a serious concern because of a high level of chemicals in food causes severe health issues. Safeguarding the public from the risk of adulterated foods has become a challenging mission. Chloropropanols are of importance to food safety and food security because they are common chemical food contaminants and believed to be carcinogenic to humans. In chemical sensing, chloropropanols are challenging analytes owing to the lacking diversity of functional groups and difficulty in targeting the hydroxyl group in aqueous environments. Moreover, because of their small molecular size, the compositions of chloropropanols remain challenging for achieving chromatographic determination. Herein, to simulate human smell and taste sensations, serum albumins, which are protein-based receptors, were introduced as low-selective receptors for differential sensing. Utilizing serum albumins, a fluorophore (PRODAN), and an additive (ascorbic acid), a differential-based optical biosensor array was developed to detect and differentiate chloropropanols. By integrating the sensor array with linear discriminant analysis (LDA), four chloropropanols were effectively differentiated based on their isomerism properties and the number of the hydroxyl groups, even at ultra-low concentration (5 nM). This concentration is far below the maximum tolerable level of 0.18 μM for chloropropanols. The sensing array was then employed for chloropropanols differentiation and quantification in the complex mixtures (e.g., synthetic soy and dark soy sauces). Leave-one-out cross-validation (LOOCV) analysis demonstrated 100% accurate classification for all tests. These results signify our differential sensing array as a practical and powerful tool to speedily identify, differentiate, and even quantify chloropropanols in food matrices.

Keywords: Chloropropanols; Differential sensing; Fluorescence; Linear discriminant analysis; Chemometrics; Serum albumins

1. Introduction

Owing to the recent growth trends in the incidence of food-contaminating outbreaks and demand for advanced food security, there is increasing attention is being paid to improving strategies for food carcinogen detection. Additionally, in the global context of food safety and quality assurance, the World Health Organization (WHO) efforts require a simplistic approach to identify and discriminate food contaminants. Therefore, cost-effective and rapid detection of food carcinogens is crucial in protecting the public from the danger of contaminated foods [1].

Chloropropanols are a group of organic chemical constituents which most probably environmental contaminants; however, they are still most frequently found in heat-processed foods (e.g., soy sauces, savory snacks, and seasoning cubes), either in a bound or free form [2]. Among the chloropropanols found in foods, 3-chloropropane-1,2-diol (3-MCPD) is the more worthy of attention on the strength of its abundance and toxicity. Additionally, 1,3-dichloropropan-2-ol (1,3-DCP) is also of interest. The above two chloropropanols are process-based food contaminants with high carcinogenicity and genotoxicity [3]. Animal-based toxicity tests have revealed that excessive consumption of 3-MCPD and 1,3-DCP for a sustained period can potentially result in kidney, reproductive organ, and liver cancers [3,4]. The available toxicity data evidenced that

both 3-MCPD and 1,3-DCP are cancer-inducing agents; therefore, they are categorized as possible human carcinogens (Group 2B) and indexed by California Proposition 65 (Prop. 65) [3]. Currently, there are a plethora of techniques used for 3-MCPD and 1,3-DCP determination, predominantly chromatography [2,5-7], electrochemistry [8], potentiometric chemosensing [9], and molecular imprinting [10,11]. However, most of these approaches involve sophisticated instrumentation as well as labor-intensive and time-consuming derivatization procedures. Consequently, it is indispensable to develop a convenient, reliable, and high-throughput advanced analytical method to simultaneously detect and quantify 3-MCPD and 1,3-DCP. This method should be able to meet the requirements of diverse practical applications and aid in the establishment of hazard analysis and critical control points (HACCP) in the food manufacturing.

Over the past few years, the applications of differential sensing have drawn tremendous interest, specifically in molecular recognition [12-15]. In comparison with highly specific receptors based on their powerful affinity to an analyte required by the classical “lock-and-key” approach, differential sensing depends on the fingerprint pattern. This pattern is basically generated by the interaction of the analyte with differential receptors having multiple binding affinities and their resulting characteristic response patterns [16,17]. The attractiveness of differential sensing originates principally from the simulation of human taste and smell sensations by an array of non-selective receptors, yielding distinctive responses for different complex mixtures or analytes as an approach for identifying flavor and aroma responses [15,17]. These biological sensations utilize protein scaffolds for targeting a range of chemical compounds [18]. Low-selective proteins, SAs with multitudinous binding sites and of approximately 66.5 kDa, are well

known to bind a diverse range of exogenous and endogenous molecules, namely toxins, pharmaceutical drugs, fluorescent probes, vitamins, hormones, bile acids, long-chain fatty acids, and terpenes [16,19,20]. Besides, SAs from differing species are believed to have remarkable dissimilarities in their amino acid sequences. This is exemplified by illustrating the 24% difference in the sequence homologies of bovine and human serum albumins [20]. SAs are also regularly used as anti-fouling biomolecules to protect (bio)sensors from non-specific interactions with biomolecules that interfere [21,22]. On those grounds, we theorized that SA could be employed as a cross-reactive receptor for differential sensing routines. As a proof-of-concept for differential sensing, we aimed for chemical substances that SAs have never been reported to bind, namely chloropropanols (Fig. 1). However, it is extremely challenging to target the alcohol functional group(s) of chloropropanols in aqueous environments using synthetic molecular receptors; as a consequence, there is a scarcity of information on chloropropanol molecular recognition and sensing [9].

Figure 1

Although the determination of chloropropanols by conventional analytical techniques is of significant for food safety, sample preparation is frequently tedious and rather lengthy. In short, classical chloropropanols detection techniques include first step derivatization of small-molecule chloropropanols, followed by identification and quantification using analytical instruments (e.g., gas chromatography–mass spectrometry). In specific, differential sensing technique has high level practicability in some real-world applications ranging from medical to environmental, such as the differentiation between healthy and metastatic tissues and the identification of harmful heavy metal ions in water

[14,17]. Taking advantage of the capability of the differential sensing technique to identify, quantify, and differentiate various analytes, a powerful sensor array capable of accurately identifying and quantifying the chloropropanols (food contaminants) in complex sample matrices before chromatographic analysis and any marketing authorization is highly demanded in food processing industrial applications. In light of this, the development of a differential-based optical sensing platform for the simultaneous detection, differentiation, and quantification of chloropropanols is firstly reported in this study. Our sensing array is composed of only three SAs: bovine, human, and rabbit serum albumins (BSA, HSA, and RSA, respectively). It is combined with a fluorescent probe (PRODAN) and an additional dopant molecule (ascorbic acid, AA), which bind differentially to SA bioreceptors, and thus forming the sensing ensemble to help enhance analyte differentiation. The target analytes (chloropropanols) are introduced, and the indicator (PRODAN) is displaced from the sensing ensemble. Thus, different fluorescence modulations are observed while also being dependent on the types of SAs. Hence, the principal objective is to determine whether chloropropanols can be distinguished by their subtle chemical structure variations, in particular, the number and structural arrangement of the hydroxyl groups (−OH). In addition, previous works have indicated that it is practical to identify, differentiate, and even quantify an analyte of interest (e.g., glycerides, cancer cells, and plasticizers) singly or in complex mixtures [13,14,23]. Therefore, the second key objective of this study is to further extend the capability of differential sensing arrays. This is ultimately with the aim of revealing that this method can be employed in differentiating chloropropanols in complex mixtures (e.g., synthetic soy sauce samples) as well as obtaining detailed information about the tested

mixtures. In this context, our present study does not have intentionality to replace the existing chromatographic methods. In contrast, it demonstrates the feasibility of using differential sensor array as a versatile technique that serves as a practical analytical screening tool to ensure the quality control of food samples. In the whole, this proposed sensing technique could meet the requirements of low-cost, ease of operation, and rapid determination.

2. Experimental section

2.1. Chemicals and materials

Sodium dihydrogen phosphate, NaH_2PO_4 (≥ 98.0%), and sodium hydrogen phosphate, Na_2HPO_4 (≥ 99.0%), were obtained from Sigma-Aldrich (St. Louis, MO, USA). Sodium azide for synthesis, NaN_3 (≥ 99.0%), was purchased from Merck (Hohenbrunn, Germany). *N*,*N*-Dimethyl-6-propionyl-2-naphthylamine, PRODAN (≥ 98.0%, high-performance liquid chromatography (HPLC) grade, Sigma-Aldrich Czech Republic), was used without further purification because no major impurities were detected on excitation at 280 nm. Essentially fatty acid- and globulin-free bovine serum albumin (BSA) and human serum albumin (HSA) as well as essentially globulin-free rabbit serum albumin (RSA) were obtained commercially from Sigma Chemicals Company (St. Louis, MO, USA). 3-MCPD (98.0%), 3-chloropropan-1-ol (98.0%), and ascorbic acid (≥ 99.0%, ACS reagent grade) were procured from Sigma-Aldrich Company (St. Louis, MO, USA). Moreover, 1,3-DCP (98.0%) and 2,3-dichloropropan-1-ol (≥ 97.0%) were obtained from Merck (Selangor, Malaysia). Methanol (≥ 99.8%,

157 HPLC grade) was supplied from Friendemann Schmidt (Washington, USA). Deionized
158 water (18.2 MΩ-cm at 25 □) was obtained from a Millipore Milli-Q Plus Water
159 Purification System (Bedford, MA, USA). Synthetic soy sauce and dark soy sauce were
160 purchased locally from a grocery store at Selangor state, Peninsular Malaysia. All of the
161 above-mentioned chemicals were used without further purification.

162

163 *2.2. Preparation of stock solutions*

164 Phosphate buffer solution (10 mM, pH 7.0) was prepared using a 1:2 molar ratios
165 of NaH_2PO_4:Na_2HPO_4 in double-distilled water. Then, 0.02% (w/v) sodium azide was
166 introduced to the prepared phosphate buffer solution as an antimicrobial agent to kill or
167 inhibit the growth of microorganisms or molds. The final phosphate buffer solution was
168 filtered prior to the experimental use. The PRODAN stock solution was prepared in
169 methanol. By the dry method, an aliquot volume of the methanolic PRODAN solution
170 was transferred to a 15-mL screw-capped vial, and subsequently dried under a stream of
171 nitrogen gas to create a thin film of PRODAN. Next, the desired amount of 10 mM
172 phosphate buffer (pH 7.0) was added to the same vial, followed by covering it with
173 aluminum foil to minimize light exposure. Finally, it was stored in the freezer (-4 □) until
174 the day of experiment. The final concentration of the PRODAN stock solution was
175 determined spectrophotometrically on a Shimadzu UV-2600 UV-Visible
176 spectrophotometer, following the Beer−Lambert law:

177 $$A = \varepsilon \times C \times l \qquad (1)$$

where A is an absorbance, ε is the molar extinction coefficient of PRODAN (ϵ_{360} = 1.80 × 10^4 M^{-1} cm^{-1}), C is the concentration of PRODAN (M), and l is the optical path length in cm. In this study, the PRODAN stock solution with a concentration of 1.11 × 10^{-6} M (~1 μM) was prepared using the dry method. The BSA, HSA, and RSA stock solutions were prepared by dissolving their respective lyophilized crystalline powders in 10 mM phosphate buffer (pH 7.0) and their concentrations were estimated spectrophotometrically at 280 nm using a Shimadzu UV-2600 UV-Visible spectrophotometer.

2.3. Fluorescence titration of PRODAN with SAs

Fluorescence assays were conducted by adding different SA stock solutions (90 μM BSA, 90 μM HSA, or 100 μM RSA) into the 10 mM phosphate buffer (pH 7.0) containing ~1 μM PRODAN solution, and thus investigating the binding ratios of the PRODAN to the SAs. Subsequently, each SA−PRODAN mixture was incubated in the dark (25 □) for 30 min prior to the fluorescence analysis. The fluorescence measurements were conducted on a Varian Cary Eclipse fluorescence spectrophotometer using Hellma® fluorescence cuvettes with dimensions of 10 × 10 mm path length. Fluorescence emission spectra were then measured at 25 □ in a wavelength range of 385–685 nm with the excitation wavelength set as 365 nm (λ_{ex} = 365 nm, λ_{em} = 385–685 nm). Both the excitation and emission bandwidths were set as 5/5 nm per step.

2.4. Determination of binding parameters between SAs and PRODAN

To determine the binding constant (K_a) of PRODAN for each serum albumin, a binding curve was plotted and fitted to a 1:1 binding ratio. Thereafter, the binding constant of PRODAN with each SA was estimated from the above binding curve using the Benesi−Hildebrand equation for a 1:1 complex formation, as expressed in the equation below.

$$I_{\mathrm{f}} = \frac{I_{\mathrm{f}}^{0} + I_{\mathrm{PRODAN-SAs}} k_1 [\mathrm{SAs}]}{1 + k_1 [\mathrm{SAs}]} \quad (2)$$

where I_{f}^{0} is the fluorescence intensity of PRODAN without the SAs and I is the fluorescence intensity when all PRODAN molecules form complexes with the SAs. For the evaluation of the number of binding sites (n) of each SA−PRODAN complex, the resulting data were fitted to the Hill equation iteratively using the Levenberg−Marquardt non-linear least squares algorithm with OriginPro 2016 software (Originlab Corporation, Northampton, MA, USA).

2.5. Chloropropanols interaction with SAs−PRODAN sensing ensembles

To reveal the binding interactions of the chloropropanols with the sensing ensembles, cuvette assays were performed. This involved titrating various chloropropanols (100 µM 3-MCPD, 100 µM 1,3-DCP, 100 µM 2,3-DCP, or 100 µM 3-CP in phosphate buffer) into a 10 mM phosphate buffer containing ~1 µM PRODAN and SAs solutions (20 µM BSA, 24.75 µM HSA, or 50 µM RSA). Subsequently, dark incubation was performed at room temperature (25 □, 30 min) for each mixture before proceeding with fluorescence spectroscopy. Similarly, cuvette assays were studied on a

Varian Cary Eclipse fluorescence spectrophotometer using Hellma® fluorescence cuvette with a 10 × 10 mm optical path length. The studied parameters were set as λ_{ex} = 365 nm, λ_{em} = 385–685 nm, and 5/20 nm slit widths. Furthermore, control experiments were conducted in a cuvette with the intention to investigate how strong the fluorescence signals of each sensing ensemble are in the absence of the SAs. These were performed by adding various chloropropanols into a 10 mM phosphate buffer (pH 7.0) containing ~1 µM PRODAN solution. The cuvette assays were then read at λ_{ex} = 365 nm, λ_{em} = 385–685 nm, and 5/20 nm slit widths. For comparative study on intrinsic fluorescence of the SAs, various PRODAN concentrations were added into the SAs (20 µM BSA, 24.75 µM HSA, or 50 µM RSA) in a 10 mM phosphate buffer. The cuvette assays were then read at λ_{ex} = 280 nm, λ_{em} = 315–575 nm, and 5/20 nm slit widths.

2.6. UV-Vis absorption spectral measurements

The absorption spectra of the SAs−PRODAN sensing ensembles with chloropropanols (e.g., 3-MCPD) were recorded on a Shimadzu UV-2600 UV-Visible spectrophotometer at room temperature (25 °C). A pair of 1 cm quartz cuvettes were used, and the spectra were measured in a wavelength range of 210–510 nm.

2.7. Development of 96-well plate sensing array

The differential sensing ensembles were then shifted to a 96-well plate assay from a cuvette assay when all the four chloropropanols investigated have led to a distinctive fluorescence variation for each chloropropanol. This enabled to effortlessly acquire the

multiple data repetitions demanded for pattern recognition. The prior probabilities of the chloropropanols were estimated in reference to the number of replicates for each chloropropanol, of which there were at a minimum of eight replicates. A cross-reactive differential sensing array was constructed by mixing the solutions of the four chloropropanols with a SA and the PRODAN solutions (three combinations: BSA−PRODAN, HSA−PRODAN, and RSA−PRODAN) in Costar 96-microtiter plates that were black polystyrene, non-treated, and round-bottomed plates (#3972). The plates were then analyzed using a BioTek Synergy H1 Hybrid Multimode Microplate Reader. To explore the potential of the sensing ensemble in distinguishing chloropropanols, the cuvette assays previously conducted with the all four chloropropanols were compared. Well plate assays were then prepared using a total volume of 300 µL with final concentrations of 20 µM BSA, 24.75 µM HSA, or 50 µMRSA; ~1 µM PRODAN; and 90 nM chloropropanols (3-MCPD, 1,3-DCP, 2,3-DCP, or 3-CP) in 10 mM phosphate buffer (pH 7.0). In this study, the studied concentration (90 nM) of four chloropropanols were well below the maximum allowable limit of 0.18 µM for chloropropanols that set by the European Union (EU). Each plate contained columns of one fluorescent probe and the fluorophore with the SAs without the chloropropanols as the controls. Eight experimental replicates were conducted for each SA/PRODAN/chloropropanol combination and control. The 96-well plates were studied at λ_{ex} = 365 ± 10 nm and λ_{em} = 522 ± 10 nm, using a top optics with a Xenon flash. For the linear discriminant analysis (LDA), multivariate data (3 SAs × 1 probe × 4 chloropropanols × 8 replicates) were statistically analyzed without any pretreatment using the chemometric program, XLSTAT version 2014 (Addinsoft Inc, NY, USA). LDA is a pattern recognition method that optimizes the

correlation between-class and within-class variance, enabling the differentiation of the response signals and distribution of the new analytes to their relevant clusters [24]. Furthermore, LDA is a supervised technique, implying that this program initially recounts the analyte class for each data point. On this account, a validation approach known as leave-one-out cross-validation (LOOCV) is frequently reported with each LDA plot with the aim of verifying the predictability and accuracy of the model [24]. In the present study, LOOCV was applied, mainly due to a small sample size in the dataset. Therefore, in each iteration, one sample was held out for testing and the remaining samples were used for training.

2.8. Enhancement of sensing array differentiation with dopant molecule

To facilitate the LDA differentiation on the F2 axis, a wide range of doping agents known to interact with the SAs were screened. It was speculated that an incorporated additional additive would interact with the SAs such that the interaction of the SAs to the chloropropanols would be distinctively impacted, thereby further altering the PRODAN binding and modulating the fluorescence signals. As has been previously reported in the literature, ascorbic acid (AA), with an association constant of 2.0−3.5 × 10^4 M^{-1} for SAs, had little modulation effect on the fluorescence signals. Yet, it was discovered to best further differentiate the analytes of interest when compared to other dopant molecules (e.g., stearic acid and bile acid) [23]. Thus, AA was opted for differentiation purposes as a potential additive. The addition of AA to the sensing ensemble was conducted by a well plate assay prepared to have final concentrations of 20 µM BSA with 300 µM AA, 24.75 µM HSA with 371.25 µMAA, or 50 µM RSA with

750 µM AA; ~1 µM PRODAN; and 90 nM chloropropanols in 10 mM phosphate buffer (pH 7.0). Each plate contained columns of the fluorophore (PRODAN) alone, the additive (AA), and the SAs−PRODAN complexes without the chloropropanols as the controls. Eight experimental replicates were performed for each SA/PRODAN/chloropropanol/AA combination and the controls. The 96-well plates were read at λ_{ex} = 365 ± 10 nm and λ_{em} = 522 ± 10 nm, using a top optics with a Xenon flash. The resulting data (3 SAs × 1 probe × 4 chloropropanols × 1 additive × 8 replicates) were examined without any pretreatment by the LDA using XLSTAT version 2014 software (Addinsoft Inc, NY, USA).

2.9. Evaluation of quantitative measurement capacity of differential sensor array

To test the ability of the differential sensor array for semi-quantitative measurements, various concentrations of the chloropropanols were taken into account. The concentrations of the SAs, PRODAN, and AA were kept constant as before, while the concentration ranges of all four chloropropanols were from 5 nM to 10 µM. The preparation of the sample solutions was similar to the aforementioned procedures in section 2.8. The 96-well plates were studied at λ_{ex} = 365 ± 10 nm and λ_{em} = 522 ± 10 nm, using a top optics with a Xenon flash. All the obtained data were processed without further pretreatment by the LDA algorithms with XLSTAT version 2014 software (Addinsoft Inc, NY, USA).

2.10. Differentiation and quantitation of chloropropanols in unknown complex mixtures

The sensing arrays were then assessed to evidence whether chloropropanols in complex mixtures could be discerned. Soy sauces are consisted of many essential chemical compositions, including Maillard reaction products, water-soluble peptides, and free amino acids. Apart from that, chloropropanols (e.g., 3-MCPD, 1,3-DCP, and 2,3-DCP) are common heat-produced contaminants potentially generated in non-fermented synthetic soy sauces made from acid-hydrolyzed vegetable protein (acid-HVP). The aroma-active and volatile compounds as well as the chloropropanols have been previously determined in soy sauces by the ubiquitous analytical methods (e.g., GC-MS) [2]. However, the existing methods are not able to simultaneously detect all four chloropropanols due to some limitations of the experimental methods. To this end, to differentiate various chloropropanols in a complex matrix, food samples (non-fermented or so-called synthetic soy sauce and dark soy sauce) were used to prepare chloropropanol-doped samples. By this means, the identities of the prevalent chloropropanols in complex mixtures could be revealed while still facilitating the differentiation of the chloropropanols present in complex mixtures. In fact, these two soy sauces can be initially differentiated by human naked eyes based on the viscosity that resulted from different manufacturing ingredients and procedures. Different stock solutions were formed for this sensing assay: (A) ~1 μM PRODAN with the SAs (20 μM BSA, 24.75 μM HSA, or 50 μM RSA) in 10 mM phosphate buffer; (B) 90 nM chloropropanols (3-MCPD, 1,3-DCP, 2,3-DCP, and 3-CP) in 10 mM phosphate buffer; (C) 90 nM chloropropanols (3-MCPD, 1,3-DCP, 2,3-DCP, and 3-CP) with synthetic soy sauce (soy sauce was diluted by 600-fold in 10 mM phosphate buffer to prevent the fluorescence signal overloading); (D) 90 nM chloropropanols (3-MCPD, 1,3-DCP, 2,3-

DCP, and 3-CP) with synthetic dark soy sauce (dark soy sauce was diluted by 600-fold in 10 mM phosphate buffer to prevent the fluorescence signal overloading); (E) AA solutions in 10 mM phosphate buffer (300 µM, 371.25 µM, and 750 µM AA with BSA, HSA, and RSA well plates, respectively). Subsequently, a well plate assay with the final volume of ~300 µL was formulated by pipetting: ~150 µL of A, ~75 µL of either B, C, or D, and ~75 µL of E. Each plate contained columns of the fluorescent probe, the additive, the chloropropanols, the soy sauce samples, as well as a column of SAs−PRODAN complexes without the chloropropanols as the controls. Each SA/PRODAN/chloropropanol/AA/sauce sample combination and the controls were replicated eight times. Similarly, the 96-well plates were studied at λ_{ex} = 365 ± 10 nm and λ_{em} = 522 ± 10 nm, using a top optics with a Xenon flash. The obtained fluorescence data (3 SAs × 1 probe × 4 chloropropanols × 1 additive × 2 sauce mixtures × 8 replicates) were statistically analyzed by the LDA technique. Note: In this study, sauce mixtures are referring to the combination of synthetic soy sauce and synthetic dark soy sauce without actually mixing these two synthetic soy sauce samples. Each synthetic soy sauce sample was added to the well. After performing microplate assay, the obtained data from both the synthetic soy sauce samples were combined and analyzed using LDA.

To study the unknown mixture, particularly soy sauce samples, the partial least squares regression (PLSR) model was employed for simultaneous quantitative analysis of the chloropropanols. The PLSR method was developed to investigate the relationship between the fluorescence spectra and the concentrations of relevant chloropropanols. The acquired data from the chloropropanol mixtures with known concentrations, ranging from 0.005−10 µM, were applied as a training dataset to establish the PLSR model. All the

data were processed using the XLSTAT version 2014 software (Addinsoft Inc, NY, USA).

2.11. Sensing array reproducibility

To ensure the reproducibility of the sensing array, the experiment was systematically replicated in its totality. Briefly, we aimed to investigate whether we would acquire virtually the same response each time an independent reiteration of the entire experiment was accomplished. This included the repetition of the differentiation study of chloropropanols in pure buffer solutions as well as in complex mixtures, beginning with the freshly prepared stock solutions of each sensing component. The experiments were repeated according to the above-mentioned experimental procedures.

3. Results and discussion

3.1. Fluorescence assays of PRODAN to SAs

In this study, fluorescence spectroscopy was performed to investigate the non-specific interactions between biological macromolecules (e.g., SAs) and small molecules possessing similar molecular structures (e.g., chloropropanols). Fig. 2a illustrates the changes in the fluorescence intensity upon binding of PRODAN to the SAs (e.g., BSA). As evidenced in Fig. 2a, upon excitation at 365 nm, PRODAN exhibits a remarkable intrinsic fluorescence with a maximum emission wavelength at 522 nm. However, there is a significant decrease in the fluorescence intensity at 522 nm on the formation of the

BSA−PRODAN complex, when increasing concentrations of BSA are added to a fixed concentration of PRODAN. Interestingly, a hypsochromic shift (blue shift) in emission is clearly noticeable on the addition of BSA to PRODAN (Fig. 2a). Moreover, an additional band appears at 465 nm, corresponding to the locally excited state of BSA-bound PRODAN. The emergence of the locally excited state reveals that PRODAN encounters a low-polarity environment in BSA. The contribution of the twisted intramolecular charge transfer band reduces with increasing BSA concentrations, whereas that of the locally excited band increases, implying that numerous PRODAN molecules bind to BSA [25]. Specifically, the formation of the new peak at 465 nm is most probably a result of the binding of PRODAN into a hydrophobic pocket on BSA. This destabilizes the charged excited state of PRODAN, resulting in a larger HOMO−LUMO (HOMO: highest occupied molecular orbital, LUMO: lowest occupied molecular orbital) gap and leading to a higher energy with a lower emission wavelength. Furthermore, the emission spectrum of the BSA−PRODAN complex is deconvoluted using a combination of log-normal functions to demonstrate the simultaneous existence of the locally excited and twisted intramolecular charge transfer species, with the fluorescence emission spectrum of PRODAN in phosphate buffer as reference (Fig. 2b). In addition, the fluorescence characteristics as observed at 465 nm could also be affected from the radiationless energy transfer between the bound PRODAN and the tryptophan residue (Trp-134) of BSA [26,27]. It is also noteworthy to mention that the existence of an isoactinic point at around 495 nm, revealing the occurrence of a single equilibrium between two emitting species (free and bound PRODAN) in the excited state. Note: The deconvolution of the spectrum was performed with the OriginPro 2016 software (Originlab Corporation,

Northampton, MA, USA), which provided the best fit for separating the contributions of the bound and free PRODAN species.

Figure 2

The binding constant of PRODAN with BSA was calculated to be (2.17 ± 0.36) × 10^5 M^{-1} after fitting the resulting data with a 1:1 binding model using non-linear regression analysis following the Benesi−Hildebrand equation (Fig. 2c). Fig. 2c is obtained from the resulting data displayed in Fig. 2a and is used to explore the concentration of PRODAN at which approximately 90% saturation occurs. The affinity constant at the studied conditions is in the order of 10^5 M^{-1}, demonstrating high-affinity interactions between PRODAN and BSA. However, in the current study, the binding constant estimated for the BSA−PRODAN complex is smaller than that previously reported in the literature (e.g., 1.00 ± 0.01 × 10^6 M^{-1}, 5.0 ± 0.3 × 10^5 M^{-1}) [19, 25]. This difference may arise from the variations in the experimental parameters (e.g., temperature, ionic strength, or pH of phosphate buffer) and also in the fatty acid content of BSA, because fatty acids and PRODAN are known to bind to sub-domain IIIA of BSA. Moreover, in this study, the estimated number of binding sites is 1.13 ± 0.13. This result discloses that PRODAN only occupies one equivalent binding site in BSA with high affinity, indicating complex formation between BSA and PRODAN in a 1:1 molecular ratio.

Interestingly, a similar phenomenon for the BSA−PRODAN interaction is also observed in the binding study of PRODAN to HSA and RSA (Fig. S1 and Fig. S2 of the Supplementary Information, SI). Based on the 1:1 stoichiometry isotherm, association

422 constants of (8.63 ± 0.60) × 10^4 M^{-1} and (7.28 ± 0.34) × 10^4 M^{-1} are obtained for binding
423 of PRODAN to HSA and RSA, respectively. These association constants revealed that
424 PRODAN had the highest affinity to interact with BSA. The affinity constants for the
425 interactions of the various SAs and PRODAN are then arranged in the following order:
426 RSA < HSA < BSA. In addition, the number of binding sites in the HSA−PRODAN and
427 RSA−PRODAN complexes are calculated to be 1.25 ± 0.08 and 1.21 ± 0.43, respectively
428 (Table S1). From these findings, it is noteworthy that the number of binding sites were
429 found to be independent of the affinity constants. This implied that PRODAN only bound
430 to one but at different binding sites in each SA, because their respective association
431 constants were different.

432

433 *3.2. Fluorescence binding titration of chloropropanols into SAs−PRODAN*
434 *differential sensing ensemble*

435 By virtue of a fluorescence technique, the interactions of the four chloropropanols
436 (3-MCPD, 1,3-DCP, 2,3-DCP, and 3-CP) are carefully monitored. The titration of the
437 chloropropanol solutions into the SAs−PRODAN differential sensing ensemble caused
438 the fluorescence intensities at 465 nm (λ_{max} for the bound PRODAN) to be increased then
439 decreased for BSA, whereas to be increased for HSA and RSA. Meanwhile, the
440 fluorescence intensities at 522 nm (λ_{max} for the free PRODAN) increased for all the SAs
441 (Note: Fig. 3 exhibits the fluorescence modulation on the addition of 3-MCPD into the
442 SAs-PRODAN sensing ensemble; Fig. S3, Fig. S4, and Fig. S5 present the fluorescence
443 modulation on the addition of 1,3-DCP, 2,3-DCP, and 3-CP into the SAs-PRODAN
444 sensing ensemble, respectively). Hence, we hypothesize that the fluorescence modulation

445 after the chloropropanol addition could be a result of indicator (bound PRODAN)
446 displacement from the hydrophobic binding pockets of the SAs, which may be expected
447 to further limit the rotor motions.

448 **Figure 3**

449 In addition, one trend noticed for the BSA−PRODAN complex is that the
450 fluorescence intensity increases upon adding the chloropropanol (Fig. 3a, Fig. S3a, Fig.
451 S4a, and Fig. S5a). This phenomenon can be explained as a result of homotropic
452 allosteric interactions between the chloropropanols and BSA in which the binding of the
453 chloropropanols within the primary binding site affect the binding characteristics of the
454 other binding sites on BSA. Subsequently, the fluorescence intensity decreases upon
455 addition of 0.15–0.25 μM chloropropanols, demonstrating that the chloropropanols are
456 competitively bound to the binding pockets of BSA (Fig. 3a, Fig. S3a, Fig. S4a, and Fig.
457 S5a). Contrastingly, the fluorescence intensity increases even on the addition of high
458 chloropropanol concentrations to the HSA−PRODAN and RSA−PRODAN complexes,
459 respectively (Fig. 3b−c, Fig. S3b−c, Fig. S4b−c, and Fig. S5b−c). This phenomenon
460 could result from the alteration in the local microenvironment of the tryptophan residue
461 (Trp-214) within the binding sites of HSA and RSA upon the chloropropanol binding.
462 This can be further explained that the chloropropanols being bound to a more
463 hydrophobic region on HSA and RSA, thus changing the polarity of the protein
464 environment and enhancing the fluorescence intensity. In brief, when high concentrations
465 of chloropropanols are introduced into the sensing system, the chloropropanols, as the
466 competitive analytes, displaced the PRODAN indicator from the binding site of SAs and
467 thus modulating the fluorescence signals. However, the fluorescence modulation is

strongly dependent on the type of SAs. Moreover, the fluorescence modulation of the BSA−PRODAN complex behaved differently from those of the HSA−PRODAN and RSA−PRODAN complexes on the addition of various chloropropanols. This could be reasonably explained by the differences in the number of tryptophan residues in these SAs. HSA and RSA have only one tryptophan residue, which is Trp-214. This tryptophan residue is well-exposed to the hydrophobic region of the SAs (less polarity region). In contrast, BSA has two tryptophan residues (Trp-134 and Trp-213). Trp-134 is well-exposed to the hydrophilic region, whereas Trp-213 is in the same region as Trp-214. Upon binding of the chloropropanols to BSA, the chloropropanols either became bound to the Trp-213 or Trp-134 residue in the binding site of BSA. Thus, the difference in fluorescence modulation might be observed. Basically, the intrinsic fluorescence of this SA was almost solely contributed by the tryptophan residue. On the interactions of the SAs−PRODAN sensing ensembles with the chloropropanols, the orientations or positions of the tryptophan residues were significantly changed, modifying their exposure to the sensing medium. This changed the fluorescence quantum yields of the SAs. Therefore, the HSA and RSA sensing ensembles exhibited distinctive fluorescence modulations to the BSA sensing ensemble on the binding of the chloropropanols. In fact, supramolecular interactions between chloropropanols and adsorbed SA scaffolds can potentially serve as the "electronic nose or tongue" for screening food contaminants (e.g., chloropropanols).

Furthermore, a few other prominent trends are remarkably observed in the fluorescence patterns upon interactions between the chloropropanols and the SAs−PRODAN differential sensing ensembles. First, all four chloropropanols depict the fluorescence variations at 522 nm (λ_{max} for the free PRODAN) in the order of RSA <

HSA < BSA, where no visible peak was observed at 522 nm for RSA. Second, 3-MCPD exhibits the minimum fluorescence modulation (the smallest change in the fluorescence intensity) (Fig. 3a−c). By contrast, 1,3-DCP and 2,3-DCP, which are regioisomers, present similar yet measurably different fluorescence signals (Fig. S3 and Fig. S4). Finally, 3-CP, the smallest chloropropanol molecule studied, displays the highest fluorescence variation (Fig. S5). Although there is no direct evidence, a high fluorescence variation is most probably associated with a high affinity of the chloropropanols to the SAs.

For control experiment, no significant fluorescence modulation is observed at the emission wavelength of 522 nm when the chloropropanols are added to the unbound PRODAN in the absence of any SAs (Fig. 3d and Fig. S6). This suggests that the PRODAN molecules are in the free form and do not interact with the chloropropanols. These results provide a conclusive proof for the roles of the SAs as a host in supramolecular binding for this differential sensing system.

Further insights into the SA microenvironment involvement in the binding of PRODAN and chloropropanols could be gained by studying the SA intrinsic fluorescence upon excitation at 280 nm (Fig. S7). The interaction of the SAs with other molecules may lead to a decrease in the fluorescence intensity (e.g., fluorescence quenching), which may proceed via the Förster resonance energy transfer (FRET) from a donor biomolecules (SAs) to an acceptor molecule (e.g., PRODAN or chloropropanols). As evidenced in Fig. S7, the emergence of an emission maxima at around 344 nm in the fluorescence spectra of all SAs can be corresponded to the existence of tryptophan residue in the subdomain IIA of all SAs. Titration of PRODAN to all SAs generated remarkable quenching in the

514 tryptophan fluorescence intensity. Such decrease in the fluorescence intensities of all SAs
515 with increasing PRODAN concentrations was suggestive of the interaction between
516 PRODAN and the SAs. The observed fluorescence quenching in the SAs fluorescence
517 can be caused by different molecular interactions, for instance, energy transfer, ground-
518 state complex formation, and molecules rearrangement [28]. Moreover, the tryptophan of
519 all SAs experiences a slight hypsochromic shift in emission wavelength (BSA: from 343
520 to 340 nm; HSA: from 344 to 341 nm; and RSA: from 343 to 341 nm). This indicated the
521 changes in the surroundings of the chromophoric groups to a less polar (more
522 hydrophobic) environment where PRODAN probe is bound to the SAs. Importantly,
523 there is no visible absorption of free PRODAN near the emission maxima at around 344
524 nm of all SAs, suggesting that the emission maximum of PRODAN (λ_{max} = 484 nm) can
525 only happen via FRET from tryptophan to PRODAN. Furthermore, there was a
526 concomitant increase in the fluorescence emission at 484 nm, which was the
527 characteristic wavelength of the bound PRODAN (Fig. S7). This occurrence could be the
528 result of radiationless energy transfer from the tryptophan residue on the SAs to the
529 bound PRODAN [27]. On top of that, an isoactinic point is noticed at around 412 nm,
530 indicating the presence of two species (bound and free PRODAN) in a single equilibrium
531 and that the quantum yields are constant over the titration.

532

533 *3.3. UV-Vis absorption spectral studies*

534 Fig. 4 illustrates the UV-Vis absorption spectra of the SAs−PRODAN sensing
535 ensembles with chloropropanols (e.g., 3-MCPD). As indicated in Fig. 4, a strong
536 absorption bands near the far-UV region (210−260 nm) characterize the absorbance due

537 to peptide bond and are called as the peak due to n−σ* transition. Besides, another sets of
538 absorption bands are obviously noticed at around 280 nm, indicating the absorbance
539 owing to the aromatic amino acids (e.g., tryptophan, tyrosine, and phenylalanine) and are
540 known as π−π* transition. Upon increasing the concentration of chloropropanols, the
541 absorbance intensities of SAs near 280 nm increase and concurrently experience a slight
542 bathochromic shift in the absorption spectra (BSA: from 277 to 280 nm; HSA: from 277
543 to 281 nm; and RSA: from 278 to 282 nm) to a longer wavelength, demonstrating the
544 interaction between the SAs−PRODAN sensing ensembles and chloropropanols and
545 forming a new complex between them. Consequently, these interactions result in the
546 unfolding and loosening of the protein backbone and reduce the hydrophobicity of the
547 microenvironment of SAs.

548 **Figure 4**

549 *3.4. Well plate assessment for differential sensing array*

550 An LDA score plot of the fluorescence emission data generated from the well
551 plate array is illustrated in Fig. 5a. The resultant score plot demonstrates two principal
552 canonical factors of 98.56 and 1.37%, exhibiting excellent differentiation near the F1 axis.
553 This thus discloses that a single discriminant function is adequate to depict the major
554 differences between the studied analytes that possess similar molecular structures. This
555 LDA model correctly classifies the four chloropropanols based on their array responses
556 with 100% accuracy, as determined by the LOOCV method (Fig. 5a−b and Table S2). In
557 addition, the LDA mapping can convert the unique fingerprints of the four
558 chloropropanols into four discernible groups attributed to each chloropropanol (Fig. 5a).
559 The four chloropropanols are assembled along the F1 axis based on their respective

fluorescence modulation as observed on the differential sensing array, with 3-CP to the far left and 3-MCPD to the far right. We speculate that 1,3-DCP and 2,3-DCP (regioisomers) are less responsive toward the differential sensing array owing to their large molecular sizes as well as steric hindrance effect when compared to the other chloropropanols. These reduce their driving forces for binding differentially to the PRODAN binding sites in the SAs. Additionally, the short distances between the eight dots acquired from eight parallel measurements in each cluster confirm the excellent repeatability characteristic of the differential sensing array.

Apart from the score plot, a loading plot can be produced to determine the contributions of the receptors in the differential sensing array to each axis, thus indicating the differential nature and cross-reactivity of the sensing array. The loading plot in Fig. 5b exhibits all the SAs−PRODAN vectors targeting toward the same direction along the F1 axis. The principal contribution of each SA is toward the affinity differences of all the chloropropanols. As can be seen in Fig. 5b, all the SAs−PRODAN vectors having a large magnitude (loading closed to 1) depicts a strong positive influence on the discriminant function along the F1 axis. This suggests that all the SAs−PRODAN receptor arrays contribute the most to the differentiation of the four chloropropanols along the F1 axis. Specifically, the four chloropropanols are differentiated based on their isomerism properties. In addition, the exploration of the LDA loading plot further reveals that the F2 axis describes a dimension mainly correlated with the BSA−PRODAN and RSA−PRODAN variables. In short, these two receptors arrays contributed the most to the F2 axis differentiation. Owing to the cross-reactive nature of the sensing array, each classification axis was determined by more than one variable. The LDA loading plot also

illustrated that the BSA−PRODAN and HSA−PRODAN factors, which pointed to one single direction on both the F1 and F2 axes, have a strong positive correlation owing to their comparable vectors. In this case, the lack of cross-reactivity between these two complexes (BSA−PRODAN and HSA−PRODAN) is identified by the truth that the score vectors are practically identical where the same chloropropanol cluster distribution along the principal axis is independent of the vector identity within the LDA score plot. Furthermore, the corresponding loading plot depicted little to no cross-reactivity for the receptor arrays because they were not widely distributed in all the quadrants of the plot. From the factor-loading plot (Fig. 5b), we concluded that the BSA−PRODAN and RSA−PRODAN complexes contributed significantly to the differentiation of the four chloropropanols along the F1 and F2 axes.

Figure 5

3.5. Improvement in F2 axis differentiation with AA

As an initial step in differentiating all the four chloropropanols using the same sensing array, the results as shown in Fig. 5a are considered satisfactory. However, we attempted to enhance the differentiation in the F2 axis of the LDA score plot in order to acquire a secondary discriminatory axis with relatively more weightage, enabling excellence differentiation for comparatively more complex samples, for instance, analyte mixtures. Therefore, AA was chosen as an additive to be incorporated in the differential sensing array in favor of increasing the differentiation power along the F2 axis while concurrently improving the cross-reactivity of the differential sensor array. Previous work has revealed that AA has two binding sites for BSA with a K_a value of 10^4 M^{-1} [29]. According to Fig. 5c, upon adding of AA to the chloropropanols, PRODAN, and SA

606 solutions, the fluorescence responses are modulated differentially to a larger extent for
607 each chloropropanol than without AA. This results in an increase in the F2 axis variance
608 of the LDA plot from 1.37 to 20.71% with the maintenance of superior differentiation
609 (LOOCV analysis afforded 100% correct classification). This LDA plot exhibits a
610 significant level of differentiation on the F2 axis, thus resulting in further discrimination
611 of 3-MCPD from the other three chloropropanols. This can possibly be explained by the
612 addition of AA leads to excellent binding of 3-MCPD on the hydrophobic binding sites of
613 the SAs. This then further explains that the unique binding of AA to the C-terminal
614 catalytic domains of the SAs via a surface adsorption mechanism, leading to the coating
615 of the protein surface. The latter induces a conformational change in the SAs, particularly
616 in their secondary structures [30]. To this end, it is most likely to facilitate the binding of
617 3-MCPD to the hydrophobic pockets of the SAs. Moreover, two influential trends are
618 clearly noticed in the same LDA plot (Fig. 5c). First, the F1 axis successfully
619 differentiates some of the chloropropanols based on their isomerism characteristic.
620 Specifically, the positional isomers, 1,3-DCP (an –OH functional group attached to the
621 second carbon atom) and 2,3-DCP (an −OH functional group attached to the first carbon
622 atom), are clearly separated on the left and right sides of the plot, respectively. Second,
623 the F2 axis discriminates the four chloropropanols by the numbers of hydroxyl groups
624 (−OH), with 3-MCPD having two hydroxyl groups projected above the *x*-axis, whereas
625 1,3-DCP, 2,3-DCP, and 3-CP consisting of only one hydroxyl group projected below the
626 *x*-axis (Fig. 1 and Fig. 5c). This LDA plot demonstrates that the differential sensing array
627 is competent to discriminate subtle differences among all four chloropropanols with the
628 maximum differentiation of the analytes occurring between the chloropropanols with

isomerism properties. Thus, the enhancement in the F2 axis differentiation is favorable to possibly further aid the differential sensing array in distinguishing composite samples. For this differential sensing array, the optimum working concentration range for the chloropropanols is found to be 0.005–10 μM, although a quantifiable fluorescence signal can still be noticed even at concentration ranges below 5 nM. Most importantly, these studied concentration ranges covered the maximum international tolerable limits established by the European Union (EU) for the chloropropanols (0.18 μM). On the other hand, high chloropropanol concentrations (>10 μM) may result in the poor differentiation due to the repetitions of a single chloropropanol may be indistinguishable from other chloropropanol clusters. However, this can be overcome by performing uniform dilution or intensity normalization/standardization to avoid concentration-caused differentiation in the LDA plot.

The loading plot in Fig. 5d illustrates all the SAs−PRODAN−AA vectors aiming toward the same direction along the F2 axis. As evidenced in Fig. 5d, the BSA−PRODAN−AA vector having a small magnitude (loading closed to 0) illustrates a weak influence on the discriminant function along the F1 axis. In addition, the examination of the loading plot extracted from the LDA demonstrates that the F1 axis (LD1) reports a dimension predominantly coordinated with the RSA−PRODAN−AA and HSA−PRODAN−AA complexes. The vectors of these two variables point in different directions, revealing a strong negative correlation (loadings closed to -1 and 1, respectively). Moreover, the loading plot reveals that these two receptor arrays have contributed significantly along the F1 axis differentiation, enabling the differentiation of the chloropropanols based on their isomerism properties. In addition, the F2 axis (LD2)

652 reveals a dimension primarily corresponding to all the variables (RSA−PRODAN−AA,
653 BSA-PRODAN−AA, and HSA−PRODAN−AA). Briefly, all these variables contributed
654 the most to the F2 axis differentiation, allowing the differentiation of four
655 chloropropanols according to the numbers of hydroxyl groups. Besides, the
656 corresponding loading plot can be used to demonstrate the cross-reactivity of these input
657 variables (BSA−PRODAN−AA, HSA−PRODAN−AA, and RSA−PRODAN−AA). As
658 can be seen in Fig. 5d, the loading plot indicated that the RSA−PRODAN−AA and
659 BSA−PRODAN−AA factors are pointed to one single direction on both the F1 and F2
660 axes. This then reveals that these two input variables (RSA−PRODAN−AA and
661 BSA−PRODAN−AA) have the same correlation direction (positively correlated to each
662 other) contributed to each classification axis. This demonstrates the low cross-reactivity
663 of the receptors in the differential sensing ensemble. In addition, the factor loading plot
664 depicted in Fig. 5d reveals significance capability of the SAs−PRODAN−AA receptors
665 accounting for the improved discriminatory ability of the differential sensing array, where
666 all the variables contribute remarkably to both the axes. These results support our
667 presumption that the addition of AA to the sensing array can further improve the
668 differentiation of the chloropropanols as well as enhance the discriminant ability of the
669 differential sensing array.

670

671 *3.6. Semi-quantitative determination of chloropropanols*

672 The semi-quantitative analysis of chloropropanols is performed at varied
673 concentrations ranging from 5 nM to 10 μM. The resulting data are analyzed by LDA and
674 the two-dimensional (2D) LDA plots are illustrated in Fig. 6. As can be seen in Fig. 6, the

four chloropropanols with diverse concentrations can trigger different fluorescence responses and therefore each LDA score plot has different tendencies depending on the concentrations. As a matter of fact, the occurrence of this phenomenon is mainly due to the supramolecular interactions (e.g., hydrogen bonding and hydrophobic interactions) between the SA−PRODAN sensing ensembles and various chloropropanols at different concentrations, thus generating different fluorescence response patterns for each concentration. Subsequently, the multidimensional fluorescence data obtained at different concentrations are evaluated using LDA technique. Consequently, the four chloropropanols at each concentration (0.005, 0.05, 0.18, 0.50, 5, and 10 μM), equivalent to that at concentration of 0.09 μM (Fig. 5c), create specific fluorescence fingerprints that can be grouped into different clusters and thus successfully demonstrating concentration-dependent discrimination (Fig. 6). The classification accuracy of each chloropropanol at each concentration is 100%. These findings significantly reveal that the developed differential sensor array has an excellent capacity to qualitatively and quantitatively detect as well as differentiate the chloropropanols over a wide range of concentrations. Importantly, these results also indicate high practicability of our differential sensor array for real-world applications, particularly in food processing industrial application, as it allows the detection of food contaminants at concentrations as low as 5 nM.

Figure 6

3.7. Differentiation and quantification of chloropropanols in unknown soy sauce samples

Next, as a real-world application, we desired to find out if the horizon of the differential sensing ensemble could be extended to distinguish these four chloropropanols

in complex mixtures (e.g., soy sauce samples) after successfully differentiating all the four chloropropanols. In this study, factory-produced synthetic soy sauce and synthetic dark soy sauce were primarily selected as these two synthetic soy sauce samples were commonly used worldwide in cooking and food preparation. Then, these two synthetic soy sauce samples were directly used as analytes in the well plate assay composing of SAs, PRODAN, and AA combinations. As now discussed, our differential sensing ensemble identifies and differentiates the four chloropropanols in the sauce samples by LDA technique. Fig. S8 illustrates the unique differentiation of the synthetic soy sauce samples in their mixture categories, with the synthetic dark soy sauce and synthetic soy sauce mixtures located on the left side and right side of the F1 axis, respectively. One interesting point about this plot is that the clusters without spiked chloropropanols (just the synthetic soy sauce sample itself) and the clusters with 2,3-DCP are situated closest to each other within each soy sauce mixture. This is in line with our earlier hypothesis that speculate 2,3-DCP showing little responsiveness toward the differential sensing ensemble, again owing to its large molecular size and steric hindrance effect, reducing the hydrophobic driving force for binding differentially to the SAs. Thus, this LDA plot also highlights the significant role of the sensing medium in differentiating the four chloropropanols in each synthetic soy sauce sample. The LDA score plot is constructed with the LOOCV analysis having 100% classification accuracy (Fig. S8 and Table S3). However, when an individual LDA score plot was drawn for each synthetic soy sauce sample, a highly unique differentiation between the chloropropanols in the mixtures was observed, where the LOOCV analysis yielded 100% accurate classification (Fig. S9, Table S4, and Table S5). Therefore, it denoted that all four chloropropanols were

triumphantly differentiated as shown in the two different synthetic soy sauce samples, revealing the discriminatory power of our newly developed differential sensing array.

Although there is no evident trend with the chloropropanol arrangement for each synthetic soy sauce sample, the differential sensing array is highly capable of differentiating the significant differences among the synthetic soy sauce sample types as well as the four chloropropanols within each synthetic soy sauce sample. Therefore, when the synthetic soy sauce sample types are considered, our differential sensing array not only prominently differentiates the synthetic soy sauce samples by four chloropropanol composition while it is still being competent to considerably differentiate by the chloropropanol identity.

To further assess the feasibility of our differential sensor array, the quantitation of chloropropanols in unknown synthetic soy sauce sample is performed based on the partial least squares regression (PLSR) model, investigating the fluorescence responses and linearity of the data. Basically, the PLSR model is developed to predict the unknown concentrations of the chloropropanols based on the fluorescence data obtained from Fig. 6, ranging from 0.005−10 μM. The predictive capability of the established PLSR model is evaluated based on the comparison between actual and predicted concentration, thus evaluating by the root mean square error (RMSE) and the coefficient of determination (also denoted as R^2). In effect, RMSE is an absolute measure of fit on how close the actual data are to the model's predicted values. Besides, RMSE is a good measure to predict the accuracy of the model's response. If the main purpose of the developed model is prediction, RMSE is the most important criterion for fit. As shown in Fig. 7, the root mean square errors (RMSEs) of the datasets are comparatively small, ranging from

744 0.1120 µM to 0.2213 µM. Lower RMSE values indicate that the regression line is close
745 to the data points, thus revealing a better fit of the model. These results demonstrate the
746 favorable performance of the established PLSR model in the prediction of the related
747 chloropropanol concentrations. Moreover, higher R^2 values (R^2 value > 0.90) for the four
748 chloropropanols are observed in the performance of the chloropropanols concentration
749 prediction with R^2 = 0.9651 for 3-MCPD, R^2 = 0.9556 for 1,3-DCP, R^2 = 0.9832 for 2,3-
750 DCP, and R^2 = 0.9532 for 3-CP. These results also indicate a good fit of experimental
751 and predicted data as a result of low discrepancy between actual and predicted
752 concentration. In light of these results, it is concluded that the PLSR predictive model
753 utilized in this study indicated a reasonably good accuracy in estimating four unknown
754 chloropropanols concentrations in the synthetic soy sauce mixture. Thus, this predictive
755 model reveals a tremendous potential in acquiring the fluorescence emission spectra as a
756 function of the chloropropanols' concentration, while expresses great accuracy of the
757 model for the prediction of unknown multi-analyte concentrations.

758 **Figure 7**

759 To evaluate the matrix interferences and practical applicability of the developed
760 PLSR model for chloropropanols determination in real food samples, our differential
761 sensor array integrated with the PLSR predictive model is employed to the synthetic soy
762 sauce and synthetic dark soy sauce. To this end, four chloropropanols with diverse
763 concentrations are spiked into the synthetic soy sauce samples. Table S6 summarizes the
764 results acquired for real food matrices using the PLSR predictive model. As can be seen
765 in Table S6, the spike recovery range is determined to be 88.8−118.2%, revealing the
766 sensor array has exhibited satisfactory results in real sample analysis. Additionally, a

767 spike-and-recovery experiments have produced an acceptable recovery range (80−120%),
768 demonstrating the matrix effect of food samples has no remarkable interference effect on
769 the simultaneous determination of chloropropanols. In this matrix effect study, method
770 validation is mainly focused on a spike-and-recovery study with the aim to verify the
771 accuracy and precision of the PLSR measurements. Thus, the differential sensor array
772 incorporated with the PLSR model is competent to simultaneously predict each
773 chloropropanol's concentration in the real sample matrices with good reliability and
774 accuracy.

775

776 *3.8. Reproducibility of sensing array*

777 The experimental reproducibility of the differential sensing array was studied and
778 the LDA score plots for these iterations are depicted in Fig. S10 and Fig. S11. The
779 relative arrangements of the four chloropropanols were substantially identical to those
780 previously reported in Fig. 5c (Fig. S10 and Fig. 5c). The reproduced results, for the
781 differentiation of four chloropropanols within complex mixtures (e.g., synthetic soy sauce
782 samples), were also essentially similar with 100% classification accuracy as determined
783 by LOOCV (Fig. S11). In light of these results, the differential sensing array was
784 concluded to be reproducible.

785

786 ## 4. Conclusions

787 To put in a nutshell, this study has demonstrated the use of low-selective or highly
788 cross-reactive serum albumins as the differential receptors for the differentiation of four

chloropropanols in combination with a PRODAN probe and ascorbic acid. The four chloropropanol identities in both pure buffer solutions and complex synthetic soy sauce mixtures can be qualitatively detected from the responses in fluorescence spectroscopy. The addition of dopant molecule (ascorbic acid) is evidenced to increase the differences in the fluorescence response changes of the serum albumins in the differential sensing array, thus increasing the F2 axis differentiation. LDA effectively differentiates the four chloropropanol analytes as well as the related synthetic soy sauce samples, even at ultra-low concentration (5 nM). In addition, quantitative analysis is confidently performed not merely for the single chloropropanol analyte but also for the complex mixtures with the integration of the PLSR model. The serum albumins with high levels of cross-reactivity significantly enhance the discriminatory ability of the differential sensor array in distinguishing the four structurally similar chloropropanols. Furthermore, in the differential sensing system, all the serum albumin receptor arrays contribute outstandingly to the differentiation of four chloropropanols. The results obtained in this study support the generality of this differential sensing technique. In short, differential sensing is a versatile technique that acts as a powerful screening tool before tedious chromatography methods are needed while reveals excellent potential in differentiating and quantifying food contaminants for food safety application. We are presently expanding the scope of the differential sensing approach to detect, discriminate, and quantify diverse analyte classes to which serum albumins have not bound previously.

Declaration of interest statement

The authors declare that they have no known competing financial interests or personal relationships that could have appeared to influence the work reported in this paper.

CRediT authorship contribution statement

Siew Fang Wong: Methodology, Formal analysis, Investigation, Writing – original draft, Visualization, Data curation, Software. **Kah Hin Low:** Formal analysis. **Sook Mei Khor:** Conceptualization, Writing – review & editing, Supervision, Project administration, Funding acquisition, Resources.

Acknowledgements

This work was financially supported by the Fundamental Research Grant Scheme (FRGS) from the Ministry of Higher Education of Malaysia (MOHE) (FP035-2019A). Besides, the authors would like to thank Associate Professor Dr. Hairul Anuar Tajuddin and Professor Dr. Saiful Anuar Karsani from the Faculty of Science for their permissions in using fluorescence spectrophotometer and microplate reader throughout this research study, respectively.

Appendix A. Supplementary data

Supplementary data to this article can be found online.

831

832 ## References

833 [1] L.A. Thompson, W.S. Darwish, Environmental chemical contaminants in food:
834 Review of a global problem, J. Toxicol. 2019 (2019) 1-14.
835 [2] B.Q. Lee, C.W. Wan Mohamed Radzi, S.M. Khor, A simultaneous derivatization of
836 3-monochloropropanediol and 1,3-dichloropropane with hexamethyldisilazane-
837 trimethylsilyl trifluoromethanesulfonate at room temperature for efficient analysis of
838 food sample analysis, J. Chromatogr. A 1432 (2016) 101-110.
839 [3] B.Q. Lee, S.M. Khor, 3-Chloropropane-1,2-diol (3-MCPD) in soy sauce: A review on
840 the formation, reduction, and detection of this potential carcinogen, Compr. Rev. Food
841 Sci. Food Saf. 14 (2015) 48-66.
842 [4] A.P. Arisseto, W.C. Silva, G.R. Scaranelo, E. Vicente, 3-MCPD and glycidyl esters in
843 infant formulas from the Brazilian market: Occurrence and risk assessment, Food Control
844 77 (2017) 76-81.
845 [5] H.Y. Chung, V.M. Ponnusamy, J.F. Jen, Determination of 3-chloropropanediol in soy
846 sauce samples by liquid phase extraction coupled with microwave-assisted derivatization
847 and high performance liquid chromatography-ultraviolet detection, Int. J. Eng. Res. 4 (4)
848 (2018) 54-61.
849 [6] S. Genualdi, P. Nyman, L. DeJager, Simultaneous analysis of 3-MCPD and 1,3-DCP
850 in Asian style sauces using QuEChERS extraction and gas chromatography-triple
851 quadrupole mass spectrometry, J. Agr. Food Chem. 65 (4) (2017) 981-985.

852 [7] G. Graziani, A. Gaspari, D. Chianese, L. Conte, A. Ritieni, Direct determination of 3-
853 chloropropanol esters in edible vegetable oils using high resolution mass spectrometry
854 (HRMS-Orbitrap), Food Addit. Contam., Part A 34 (11) (2017) 1893-1903.
855 [8] X. Sun, L. Zhang, H. Zhang, H. Qian, Y. Zhang, L. Tang, Z. Li, Development and
856 application of 3-chloro-1,2-propandiol electrochemical sensor based on a
857 polyaminothiophenol modified molecularly imprinted film, J. Agr. Food Chem. 62 (20)
858 (2014) 4552-4557.
859 [9] M.K.P. Leung, B.K.W. Chiu, M.H.W. Lam, Molecular sensing of 3-chloro-1,2-
860 propanediol by molecular imprinting, Anal. Chim. Acta 491 (1) (2003) 15-25.
861 [10] M. Fang, L. Zhou, H. Zhang, L. Liu, Z.-Y. Gong, A molecularly imprinted
862 polymers/carbon dots-grafted paper sensor for 3-monochloropropane-1,2-diol
863 determination, Food Chem. 274 (2019) 156-161.
864 [11] X. Qiu, X.-Y. Xu, Y. Liang, H. Guo, The molecularly imprinted polymer supported
865 by anodic alumina oxide nanotubes membrane for efficient recognition of
866 chloropropanols in vegetable oils, Food Chem. 258 (2018) 295-300.
867 [12] E.V. Anslyn, Supramolecular analytical chemistry, J. Org. Chem. 72 (3) (2007) 687-
868 99.
869 [13] K.L. Diehl, M.A. Ivy, S. Rabidoux, S.M. Petry, G. Muller, E.V. Anslyn, Differential
870 sensing for the regio- and stereoselective identification and quantitation of glycerides,
871 Proc. Natl. Acad. Sci. U. S. A. 112 (30) (2015) E3977-E3986.
872 [14] A.M. Gade, M.K. Meadows, A.D. Ellington, E.V. Anslyn, Differential array sensing
873 for cancer cell classification and novelty detection, Org. Biomol. Chem. 15 (46) (2017)
874 9866-9874.

[15] J.J. Lavigne, E.V. Anslyn, Sensing a paradigm shift in the field of molecular recognition: From selective to differential receptors, Angew. Chem., Int. Ed. Engl. 40 (17) (2001) 3118-3130.

[16] C.J. Kubarych, M.M. Adams, E.V. Anslyn, Serum albumins as differential receptors for the discrimination of fatty acids and oils, Org. Lett. 12 (21) (2010) 4780-4783.

[17] S.-F. Wong, S.M. Khor, State-of-the-art of differential sensing techniques in analytical sciences, TrAC, Trends Anal. Chem. 114 (2019) 108-125.

[18] D. Jones, R. Reed, Golf: An olfactory neuron specific-G protein involved in odorant signal transduction, Science 244 (4906) (1989) 790-795.

[19] M.M. Adams, E.V. Anslyn, Differential sensing using proteins: Exploiting the cross-reactivity of serum albumin to pattern individual terpenes and terpenes in perfume, J. Am. Chem. Soc. 131 (47) (2009) 17068-17069.

[20] B. Friedrichs, Th. Peters Jr., All about Albumin: Biochemistry, Genetics, and Medical Applications, Academic Press Inc., San Diego, California, 1996.

[21] M. Stobiecka, A. Chalupa, B. Dworakowska, Piezometric biosensors for anti-apoptotic protein survivin based on buried positive-potential barrier and immobilized monoclonal antibodies, Biosens. Bioelectron. 84 (2016) 37-43.

[22] M. Stobiecka, M. Hepel, Effect of buried potential barrier in label-less electrochemical immunodetection of glutathione and glutathione-capped gold nanoparticles, Biosens. Bioelectron. 26 (8) (2011) 3524-3530.

[23] M.A. Ivy, L.T. Gallagher, A.D. Ellington, E.V. Anslyn, Exploration of plasticizer and plastic explosive detection and differentiation with serum albumin cross-reactive arrays, Chem. Sci. 3 (6) (2012) 1773-1779.

[24] S. Stewart, M.A. Ivy, E.V. Anslyn, The use of principal component analysis and discriminant analysis in differential sensing routines, Chem. Soc. Rev. 43 (1) (2014) 70-84.

[25] R. Thakur, A. Das, A. Chakraborty, Interaction of human serum albumin with liposomes of saturated and unsaturated lipids with different phase transition temperatures: A spectroscopic investigation by membrane probe PRODAN, RSC Adv. 4 (28) (2014) 14335-14347.

[26] M. Hosokawa, Y. Hoshino, Y. Nishikawa, T. Hirose, D.H. Yoon, T. Mori, T. Sekiguchi, S. Shoji, H. Takeyama, Droplet-based microfluidics for high-throughput screening of a metagenomic library for isolation of microbial enzymes, Biosens. Bioelectron. 67 (2015) 379-385.

[27] F.n. Moreno, J. González-Jiménez, Binding of the promen fluorescent probe to human serum albumin, Chem.-Biol. Interact. 121 (3) (1999) 237-252.

[28] H. Xu, R. Wallace, M. Hepel, Interactions of antifouling monolayers: Energy transfer from excited albumin molecule to phenol red dye, Chem. Pap. 69 (1) (2015) 227-236.

[29] X. Li, G. Wang, D. Chen, Y. Lu, Binding of ascorbic acid and α-tocopherol to bovine serum albumin: A comparative study, Mol. BioSyst. 10 (2) (2014) 326-337.

[30] M. Stobiecka, M. Hepel, J. Radecki, Transient conformation changes of albumin adsorbed on gold piezoelectrodes, Electrochim. Acta 50 (25-26) (2005) 4873-4887.

Highlights

- A differential-based optical biosensor array is developed to detect and differentiate four chloropropanols.
- Serum albumins are introduced as low-selective receptors for differential sensing.
- Differential optical biosensor array distinguishes soy sauce samples based on their mixture types and chloropropanol compositions.
- Semi-quantitative analysis via LDA shows good cluster separation for all chloropropanols at various concentrations.
- PLSR model is applied to predictively quantify the chloropropanols concentration in unknown soy sauce samples.

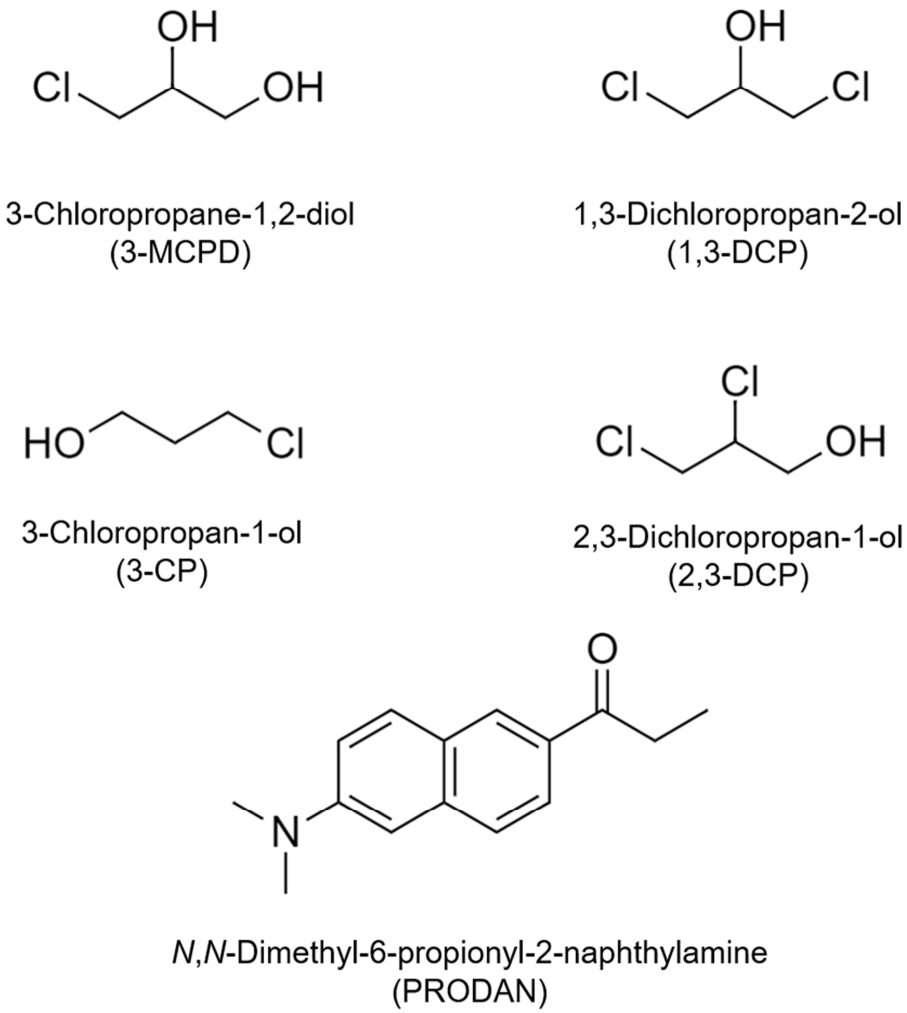

Fig. 1. Chemical structures of four chloropropanol analytes and fluorophore.

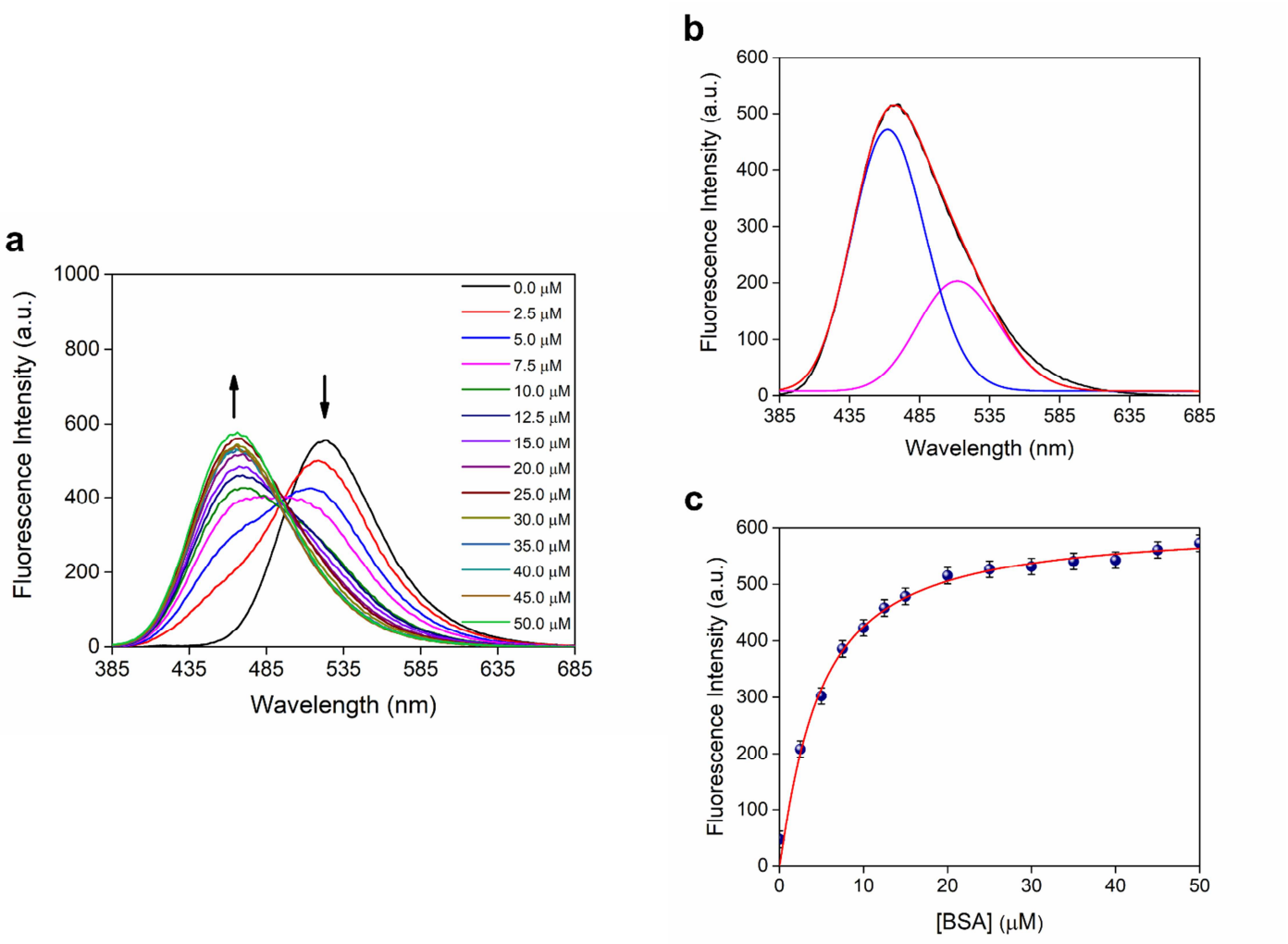

Fig. 2. (a) Titration of BSA (0.0–50.0 µM) to PRODAN (~1 µM) in 10 mM phosphate buffer (pH 7.0, 0.02% NaN_3), λ_{ex} = 365 nm, λ_{em} = 385–685 nm, and 5/5 nm slit widths. (b) The emission spectrum of PRODAN in the presence of 20 µM BSA that has been deconvoluted in the locally excited (blue line) and twisted intramolecular charge transfer (pink line) state. (c) The fitted binding curve between PRODAN and BSA, fitting to a 1:1 binding ratio at λ_{em} = 465 nm from the data shown in Figure 2a, following equation 2 and calculating a K_a value of $(2.17 \pm 0.36) \times 10^5$ M^{-1}.

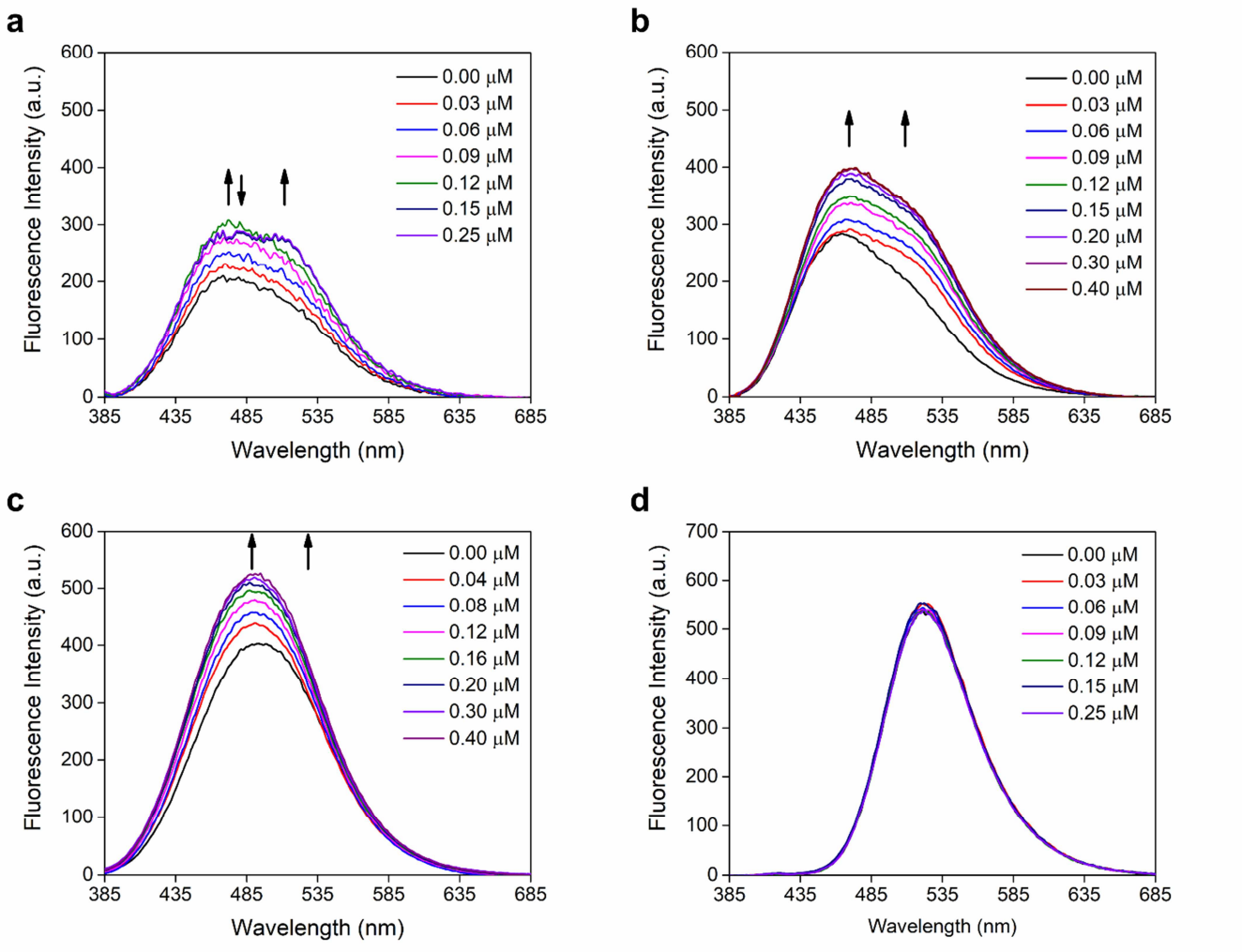

Fig. 3. (a) Titration of 3-MCPD (0.00–0.25 μM) to 20 μM BSA and ~1 μM PRODAN in 10 mM phosphate buffer (pH 7.0, 0.02% NaN_3). (b) Titration of 3-MCPD (0.00–0.40 μM) to 24.75 μM HSA and ~1 μM PRODAN in 10 mM phosphate buffer (pH 7.0, 0.02% NaN_3). (c) Titration of 3-MCPD (0.00–0.40 μM) to 50 μM RSA and ~1 μM PRODAN in 10 mM phosphate buffer (pH 7.0, 0.02% NaN_3). (d) Titration of 3-MCPD (0.00–0.25 μM) to ~1 μM PRODAN in 10 mM phosphate buffer (pH 7.0, 0.02% NaN_3). The studied parameters are set as λ_{ex} = 365 nm, λ_{em} = 385–685 nm, and 5/20 nm slit widths. Note: the above-mentioned concentration ranges of chloropropanols are selected for the reason that

these concentration ranges adequately worked well for the developed differential sensing array after studying at various concentrations. Notably, these concentration ranges covered the international maximum permissible limits for chloropropanols (3-MCPD, 1,3-DCP, and 2,3-DCP: 0.02 mg/kg; 3-CP: no maximum limit is set) that set by the European Union.

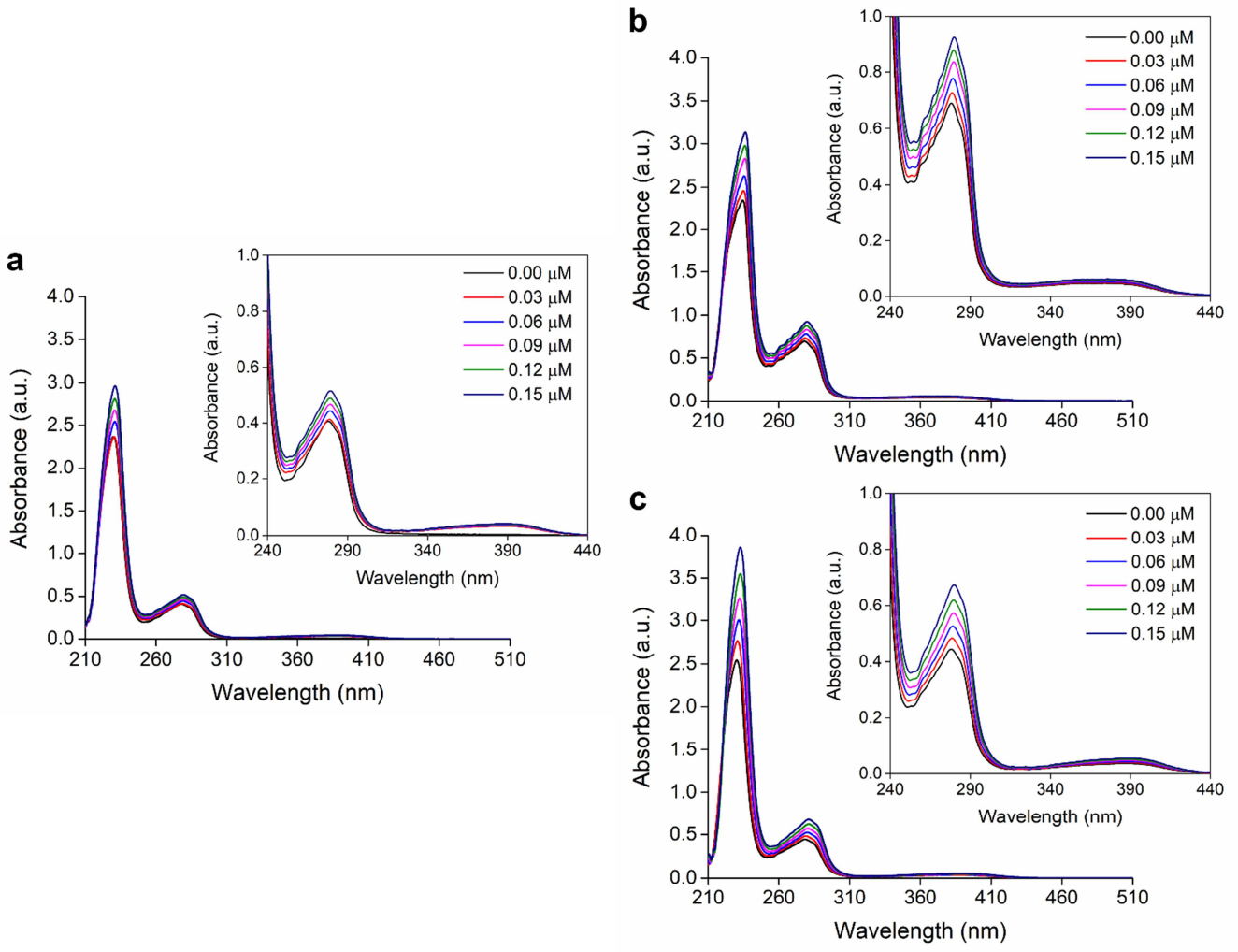

Fig. 4. UV-Vis absorption spectra of (a) 20 µM BSA, (b) 24.75 µM HSA, and (c) 50 µM RSA in the presence of ~1 µM PRODAN and 0.00−0.15 µM chloropropanols (e.g., 3-MCPD). Inset: The enlarged part of the UV-Vis absorption spectra in a wavelength range of 240−440 nm.

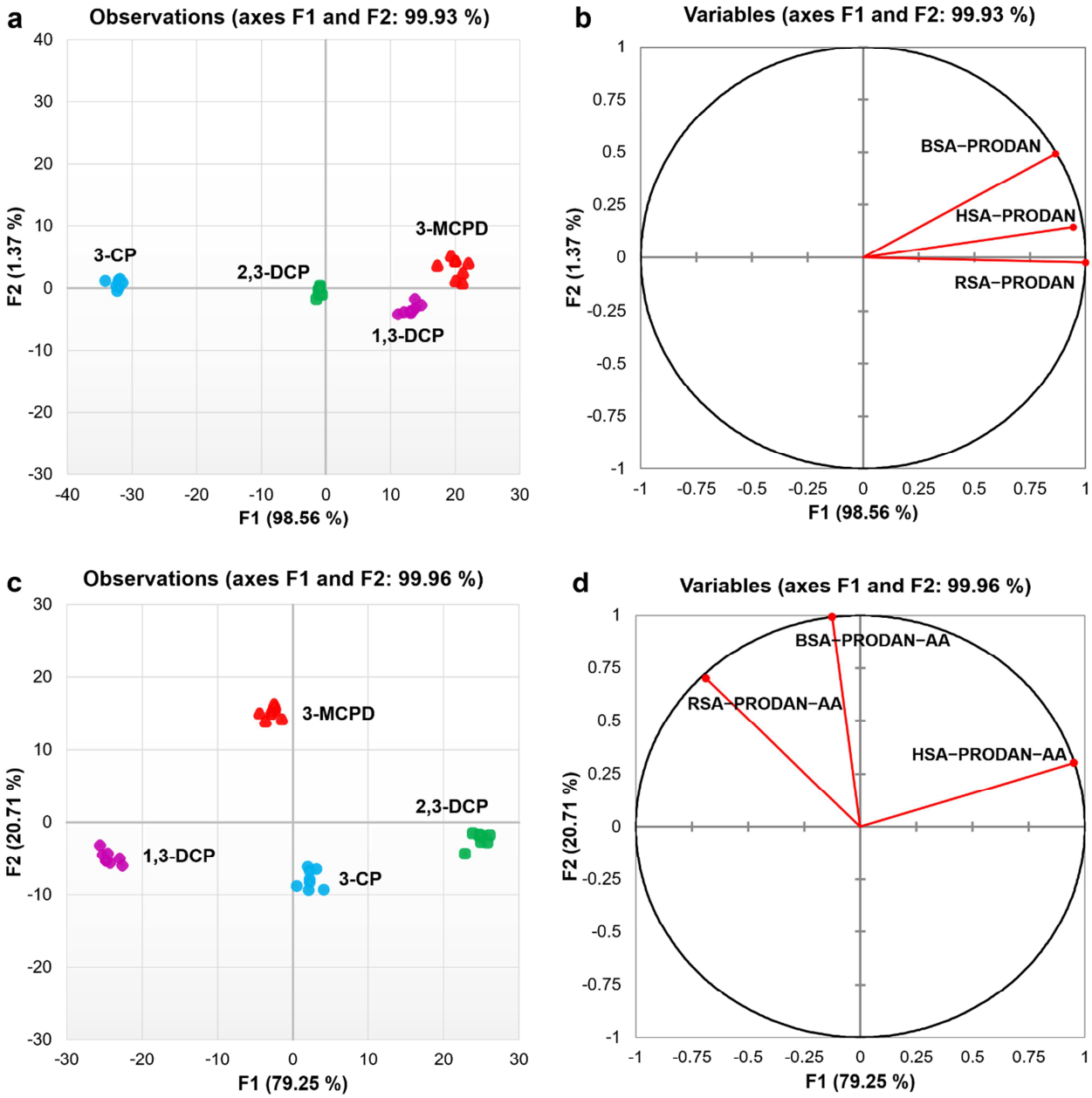

Fig. 5. (a) Linear discriminant analysis (LDA) score plot for the differentiation of the four chloropropanols. Data recorded from a 96-well plate reader with the fluorescence parameters of λ_{ex} = 365 ± 10 nm, λ_{em} = 522 ± 10 nm, and a top optics with a Xenon flash. The array compositions composed of 20 µM BSA, 24.75 µM HSA, or 50 µM RSA, ~1

μM PRODAN, and 90 nM chloropropanols in 10 mM phosphate buffer (pH 7.0, 0.02% NaN_3). (b) The loading plot of the fluorescence response pattern of the four chloropropanols using PRODAN and SAs (BSA, HSA, RSA) with the LOOCV analysis of 100% classification. The vectors on the loading plot express SAs−PRODAN contribution to the differential sensing array. (c) LDA score plot for the differentiation of the four chloropropanols with AA additions. Data acquired from a 96-well plate reader with the fluorescence parameters of λ_{ex} = 365 ± 10 nm, λ_{em} = 522 ± 10 nm, and a top optics with a Xenon flash. The array compositions constructed of 20 μM BSA with AA (300 μM), 24.75 μM HSA with AA (371.25 μM), or 50 μM RSA with AA (750 μM), ~1 μM PRODAN, and 90 nM chloropropanols in 10 mM phosphate buffer (pH 7.0, 0.02% NaN_3). (d) The loading plot of the fluorescence response pattern of the four chloropropanols using PRODAN, AA, and SAs (BSA, HSA, RSA) with the LOOCV analysis of 100% classification. The vectors on the loading plot indicate SAs−PRODAN−AA contribution to the differential sensing ensemble.

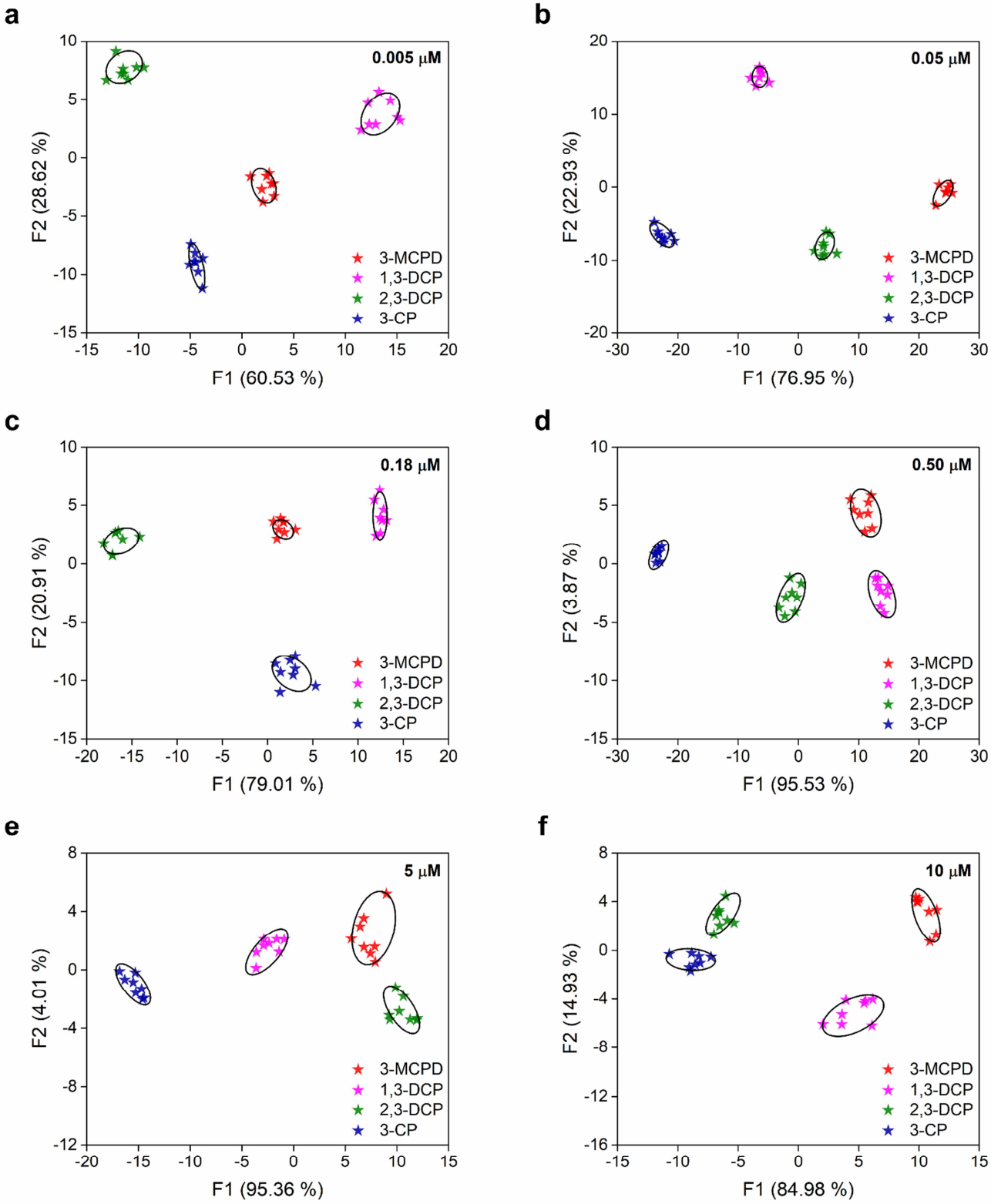
a
0.005 μM
F2 (28.62 %)
F1 (60.53 %)
b
0.05 μM
F2 (22.93 %)
F1 (76.95 %)
c
0.18 μM
F2 (20.91 %)
F1 (79.01 %)
d
0.50 μM
F2 (3.87 %)
F1 (95.53 %)
e
5 μM
F2 (4.01 %)
F1 (95.36 %)
f
10 μM
F2 (14.93 %)
F1 (84.98 %)
3-MCPD
1,3-DCP
2,3-DCP
3-CP

Fig. 6. The results of semi-quantitative determination via LDA reveal a good cluster separation for all four chloropropanols at (a) 0.005 µM, (b) 0.05 µM, (c) 0.18 µM, (d) 0.50 µM, (e) 5 µM, and (f) 10 µM, respectively. Note: 0.18 µM is indicative of the international maximum tolerable concentration for chloropropanols that established by the EU.

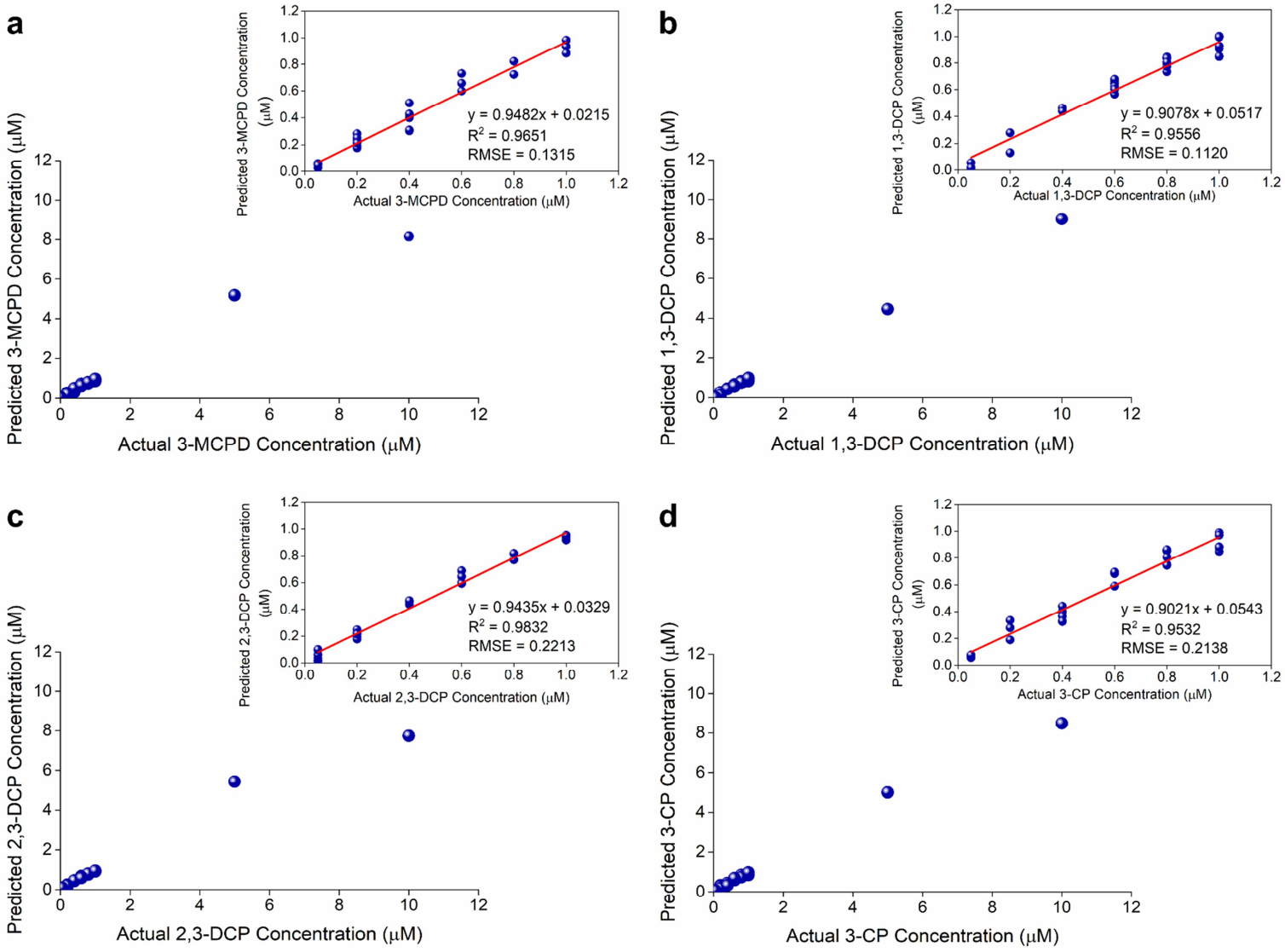

Fig. 7. The plots of actual concentration versus predicted concentration of (a) 3-MCPD, (b) 1,3-DCP, (c) 2,3-DCP, and (d) 3-CP in the sauce mixture using the partial least squares regression (PLSR) model. Inset: The enlarged part of the plots of actual concentration versus predicted concentration of chloropropanols in the concentration range of 0.005−1 μM.